Available online at www.sciencedirect.com
ScienceDirect
International Journal of Thermal Sciences 48 (2009) 226–233
International Journal of Thermal Sciences
www.elsevier.com/locate/ijts

Collision modeling between two non-Brownian particles in multiphase flow

C. Veeramani [a,*], P.D. Minev [b], K. Nandakumar [c,d]

[a] *Department of Chemical and Materials Engineering, University of Alberta Edmonton, Alberta, T6G 2G6, Canada*
[b] *Department of Mathematical and Statistical Sciences, University of Alberta Edmonton, Alberta, T6G 2G1, Canada*
[c] *Chemical Engineering Program, The Petroleum Institute, P.O. Box 2533, Abu Dhabi, UAE*
[d] *SCUT, Guangzhou, Peoples Republic of China*

Received 17 July 2007; received in revised form 8 January 2008; accepted 9 January 2008

Available online 8 February 2008

Abstract

In this paper, we develop a collision model for particle–particle and particle–wall interaction inside fluid medium based on stereomechanical impact model. One of the important parameters identified in literature that characterizes the interaction is the Stokes number (*St*), which is the ratio of the particles inertia and fluid viscosity. In dry air collisions, the coefficient of restitution (e) and coefficient of friction (f) are used to describe post-collision velocities on the basis of pre-collision velocities. In the case of collisions in fluid medium, we use the experimental results that provide the co-relation between the values of e and f as a function of the Stokes number. The collision models developed here are used in our direct numerical simulation of particulate flows to verify the model with some of the well-known behavior of particle interaction in fluids.

Keywords: Stereomechanical impact; Particulate flow; Collision; Multiphase

1. Introduction

The multiple-body collision problem is quite challenging due to the time and space resolution required to resolve the collision process. The type of interaction inside a viscous medium can change depending on the inertia of the particle and the inertia and viscosity of the fluid. While the ratio of the fluid inertial force to viscous force is captured by the Reynolds number (*Re*), in order to model the particle inertia, we need to include the dimensionless parameter called Stokes number (*St*), which is the product of density ratio of particle to fluid and the Reynolds number.

In a sufficiently viscous medium, the hydrodynamic interaction force due to the approaching particles starts acting well ahead of the actual contact; if at all any occurs subsequently. If the Stokes number is quite low, the momentum of the particles could be completely dissipated by the viscous force of the intervening fluid. The particles never come in contact. In this case, a Stokesian dynamics based model can be used to estimate the motion of the fluid. The hydrodynamic force and torque of the fluid on the particles is used to determine their further course. While this kind of modeling works well for smooth particles, rough particles on the other hand may actually come in contact due to their surface perturbations [1,2]. At sufficiently higher Stokes numbers, the particles come into contact because the fluid is not able to completely dissipate their momentum. In between the extremes of Stokesian dynamics and rigid body dynamics a range of possibilities exist. In this article, we focus on collision modeling based on rigid body dynamics [3] with correction for presence of fluid suggested by experimental results of [4].

2. Analysis and modeling

2.1. Stereomechanical impact based model

A two body interaction model is first developed for collision between two spheres based on the graphical approach of [3] for

* Corresponding author. Tel.: +1 780 492 7740; fax: +1 780 492 2881.
E-mail addresses: veeramani@ualberta.ca (C. Veeramani), minev@ualberta.ca (P.D. Minev), nkrishnaswamy@pi.ac.ae (K. Nandakumar).

1290-0729/$ – see front matter
doi:10.1016/j.ijthermalsci.2008.01.005

Nomenclature

a, b, c	co-ordinates	m	
C	relative compression velocity	$\mathrm{m\,s^{-1}}$	
d_p	particle diameter	m	
e	coefficient of restitution		
f	coefficient of friction		
G	center of gravity	m	
m^*	reduced mass $m^* = (\frac{1}{m_1} + \frac{1}{m_2})^{-1}$	kg	
$\mathbf{P}$	impulse	$\mathrm{kg\,m\,s^{-1}}$	
Q	image point		
R^*	reduced radius $R^* = (\frac{1}{R_1} + \frac{1}{R_2})^{-1}$	m	
Re	Reynolds number $Re = \frac{2R_1\rho_1 U_c}{\mu}$		
S	relative sliding velocity	$\mathrm{m\,s^{-1}}$	
St	Stokes number $St = \frac{m^*(\mathbf{U}_1 - \mathbf{U}_2)}{6\pi\mu R^{*2}}$		
U_c	characteristic velocity	$\mathrm{m\,s^{-1}}$	
U_n	dimensionless normal approach velocity	$\mathrm{m\,s^{-1}}$	
$\mathbf{X}_w$	position of closest point on wall	m	

Greek symbols

α	friction angle	rad
γ	critical angle	rad
ρ_p	density of the settling particle	$\mathrm{kg\,m^{-3}}$
θ_s	sliding direction	rad
$\boldsymbol{\omega}$	particle angular velocity	$\mathrm{rad\,s^{-1}}$

Subscripts

0	initial condition
1	first particle
2	second particle
a	approach phase
r	restitution phase

two body impact in three dimensions. Stereomechanical theory of impact is an abstract model that does not account for any stress waves originating at point of contact or any deformation of the impacting bodies. Since we model rigid bodies, the complication due to deformation is not involved. Further our particles are spherical; we need not worry about vibrations [3, p. 4]. Therefore this theory perfectly suits our purpose for modeling collision between two particles. The entire process of collision is analyzed in two phases: approach/compression phase and restitution phase. The extent of recovery after collision determines the conversion of energy stored in the body during compression phase of collision to kinetic energy during restitution phase of collision. The energy loss is captured by defining the effective coefficient of restitution (e) as follows:

$$e = -\frac{\mathbf{U}_{r1} - \mathbf{U}_{r2}}{\mathbf{U}_{a1} - \mathbf{U}_{a2}} \tag{1}$$

where $\mathbf{U}_{r1}$ and $\mathbf{U}_{r2}$ are velocities after collision and $\mathbf{U}_{a1}$ and $\mathbf{U}_{a2}$ are velocities before collision for particles 1 and 2, respectively. $e = 1$ means complete recovery or elastic collision and $e = 0$ means no recovery or plastic collision, i.e. the particles stick after collision. In general, this definition is applied only to the component of the velocities that is normal to contacting surfaces. To resolve tangential components the coefficient of friction (f) is introduced. The values of these parameters depend on the materials that are taking part in the collision and therefore must be determined from experiments. This is the major drawback of this model. The submerged particle collision experiments of [4] provide some experimental correlations for normal coefficient of restitution as a function of impact angles in three different ranges of Stokes number and the submerged pendulum experiments of [5,6] provide values for frictional coefficients. However, these experimental results do not cover the entire range of impact angles 0–90° or the entire range of Stokes numbers. There are difficulties in finding coefficients of restitution at lower range of Stokes number stemming from the fact that this range belongs to the dynamics of fluid. [4] have found in their experiments that the target sphere starts to move before the collision, making the estimation of coefficient of restitution obtained in the low Stokes number regime unreliable. The elastohydrodynamic theory developed by [7] has been shown to fit the experimental data by [8] fairly well. They arrived at a simple relationship between coefficient of restitution and Stokes number as follows:

$$e_{\mathrm{wet}} = \begin{cases} e_{\mathrm{dry}}(1 - \frac{St_c}{St}), & St > St_c \\ 0, & St < St_c \end{cases} \tag{2}$$

The value of critical Stokes number is dependent on material properties. In general, the critical Stokes number is found to be 10 [5] and e_{dry} values for various materials have been compiled by [9] based on the bouncing height of various balls on a flat plane. The Stokes number is defined as:

$$St = \frac{m^*(\mathbf{U}_1 - \mathbf{U}_2)}{6\pi\mu R^{*2}} \tag{3}$$

In terms of dimensionless quantities the Stokes number can be written as:

$$St = \frac{1}{9} Re\, U_n \frac{\rho_p}{\rho} \frac{(1 + \frac{R_1}{R_2})^2}{(1 + \frac{m_1}{m_2})} \tag{4}$$

U_n is the dimensionless relative approach velocity of the particles or a particle towards wall. For collision with a massive plane wall the factors with radius and mass ratio drops out.

2.2. Two sphere impact in three dimensions

Fig.1 shows the velocities involved in three-dimensional impact of two spheres. With reference to the figure, the linear and angular momentum equations can be written as follows.

For particle 1:

$$m_1(\mathbf{U}_{1,x} - \mathbf{U}_{1,x0}) = -\mathbf{P}_x \tag{5}$$

$$m_1(\mathbf{U}_{1,y} - \mathbf{U}_{1,y0}) = -\mathbf{P}_y \tag{6}$$

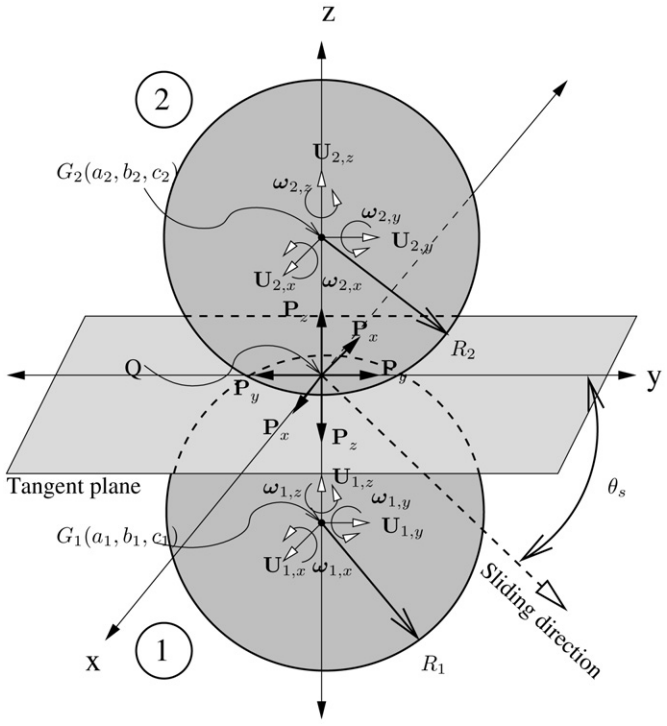

Fig. 1. Impact of two spheres in three-dimensional motion.

$$m_1(\mathbf{U}_{1,z} - \mathbf{U}_{1,z0}) = -\mathbf{P}_z \tag{7}$$

$$\frac{2}{5}m_1R_1^2(\boldsymbol{\omega}_{1,x} - \boldsymbol{\omega}_{1,x0}) = R_1\mathbf{P}_y \tag{8}$$

$$\frac{2}{5}m_1R_1^2(\boldsymbol{\omega}_{1,y} - \boldsymbol{\omega}_{1,y0}) = -R_1\mathbf{P}_x \tag{9}$$

$$\frac{2}{5}m_1R_1^2(\boldsymbol{\omega}_{1,z} - \boldsymbol{\omega}_{1,z0}) = 0 \tag{10}$$

For particle 2:

$$m_2(\mathbf{U}_{2,x} - \mathbf{U}_{2,x0}) = \mathbf{P}_x \tag{11}$$

$$m_2(\mathbf{U}_{2,y} - \mathbf{U}_{2,y0}) = \mathbf{P}_y \tag{12}$$

$$m_2(\mathbf{U}_{2,z} - \mathbf{U}_{2,z0}) = \mathbf{P}_z \tag{13}$$

$$\frac{2}{5}m_2R_2^2(\boldsymbol{\omega}_{2,x} - \boldsymbol{\omega}_{2,x0}) = R_2\mathbf{P}_y \tag{14}$$

$$\frac{2}{5}m_2R_2^2(\boldsymbol{\omega}_{2,y} - \boldsymbol{\omega}_{2,y0}) = -R_2\mathbf{P}_x \tag{15}$$

$$\frac{2}{5}m_2R_2^2(\boldsymbol{\omega}_{2,z} - \boldsymbol{\omega}_{2,z0}) = 0 \tag{16}$$

It is assumed that spheres can freely pivot around the contact point, so there is no change in the angular velocity in normal direction. The relative velocities of body 1 with respect to body 2 are:

$$\begin{bmatrix} S\cos\theta_s \\ S\sin\theta_s \\ C \end{bmatrix} = \begin{bmatrix} \mathbf{U}_{1,x} - \mathbf{U}_{2,x} + R_2\boldsymbol{\omega}_{2,y} + R_1\boldsymbol{\omega}_{1,y} \\ \mathbf{U}_{1,y} - \mathbf{U}_{2,y} - R_2\boldsymbol{\omega}_{2,x} - R_1\boldsymbol{\omega}_{1,x} \\ \mathbf{U}_{1,z} - \mathbf{U}_{2,z} \end{bmatrix} \tag{17}$$

The initial sliding velocities S_0, C_0 and the sliding direction θ_0 are determined by substituting initial velocities in the above equations. The sliding velocities in terms of impulses are obtained as follows:

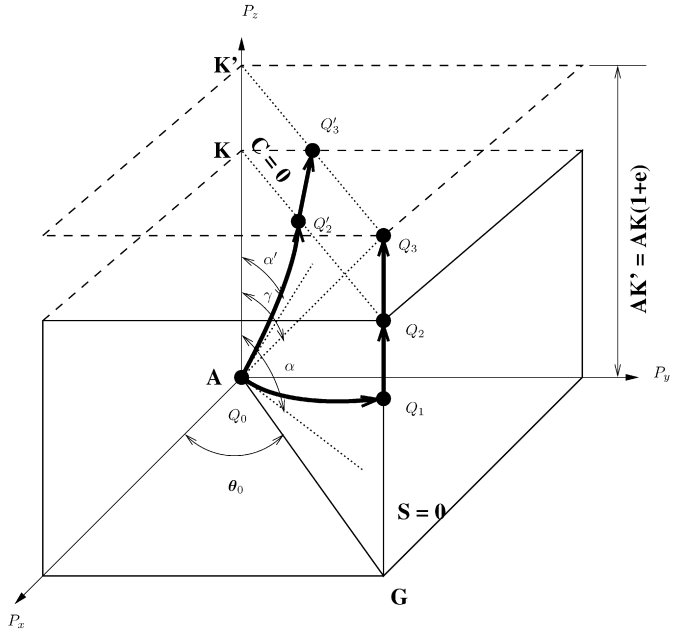

Fig. 2. Image point in three-dimensional impact between two spheres.

$$S_0\cos\theta_0 - S\cos\theta_s = \frac{7}{2}\left(\frac{m_1+m_2}{m_1m_2}\right)\mathbf{P}_x \tag{18}$$

$$S_0\sin\theta_0 - S\sin\theta_s = \frac{7}{2}\left(\frac{m_1+m_2}{m_1m_2}\right)\mathbf{P}_y \tag{19}$$

$$C_0 - C = \left(\frac{m_1+m_2}{m_1m_2}\right)\mathbf{P}_z \tag{20}$$

The planes for no-sliding and maximum compression are:

$$S = 0: \quad \mathbf{P}_x = \frac{2}{7}\left(\frac{m_1m_2}{m_1+m_2}\right)S_0\cos\theta_0 \tag{21}$$

$$\mathbf{P}_y = \frac{2}{7}\left(\frac{m_1m_2}{m_1+m_2}\right)S_0\sin\theta_0 \tag{22}$$

$$C = 0: \quad \mathbf{P}_z = \left(\frac{m_1m_2}{m_1+m_2}\right)C_0 \tag{23}$$

In Fig. 2, we show the three dimensional version of the image point trajectory in impulse space when the angle of sliding is fixed as θ_0. The planes of no-sliding (thin solid lines) and maximum compression (thin dashed lines) are also shown. The plane for termination of impact is added parallel to $C = 0$ plane. The normal impulse at termination of impact will be $(1 + e)$ times the normal impulse at the maximum compression plane. This relationship results from the definition of the coefficient of restitution (e). The relevant lengths are:

$$AG = \frac{2}{7}\left(\frac{m_1m_2}{m_1+m_2}\right)S_0 \tag{24}$$

$$AK = \left(\frac{m_1m_2}{m_1+m_2}\right)C_0 \tag{25}$$

$$AK' = \left(\frac{m_1m_2}{m_1+m_2}\right)C_0(1+e) \tag{26}$$

The critical angle γ as shown in Fig. 2 is given by:

$$\tan\gamma = \frac{AG}{AK'} = \frac{2S_0}{7C_0(1+e)} \tag{27}$$

The impulses at the image point Q, follow the curve (shown with thick solid arrows) defined by frictional impulses available. This curve will be a straight line in our case because we are assuming constant coefficient of friction (f). If friction is assumed to act at limiting value initially, then the path from Q_0 to Q_1 is described by the line:

$$\frac{\mathrm{d}P_x}{\cos\theta_s} = \frac{\mathrm{d}P_y}{\sin\theta_s} = \frac{\mathrm{d}P_z}{1/f} \tag{28}$$

Depending on the value of friction angle (α), the following two situations can arise:

(a) $f = \tan\alpha > \tan\gamma$: Friction is acting at limiting value right from the start of sliding. The image point follows the curve described by Eq. (28) from Q_0 to point Q_1 which lies on the no-sliding line. Then it reaches maximum compression plane at Q_2 and finally termination of impact at Q_3. The impulses at the termination point are:

$$\mathbf{P}_{x,3} = \frac{2}{7}\left(\frac{m_1 m_2}{m_1+m_2}\right) S_0 \cos\theta_0 \tag{29}$$

$$\mathbf{P}_{y,3} = \frac{2}{7}\left(\frac{m_1 m_2}{m_1+m_2}\right) S_0 \sin\theta_0 \tag{30}$$

$$\mathbf{P}_{z,3} = \left(\frac{m_1 m_2}{m_1+m_2}\right) C_0(1+e) \tag{31}$$

The final velocities at termination can be obtained by substituting the above impulses into impulse-momentum equation.

For particle 1:

$$\mathbf{U}_{1,x} = \mathbf{U}_{1,x0} - \frac{2}{7(1+M)}(S_0\cos\theta_0) \tag{32}$$

$$\mathbf{U}_{1,y} = \mathbf{U}_{1,y0} - \frac{2}{7(1+M)}(S_0\sin\theta_0) \tag{33}$$

$$\mathbf{U}_{1,z} = \mathbf{U}_{1,z0} - \frac{(1+e)}{(1+M)} C_0 \tag{34}$$

$$\boldsymbol{\omega}_{1,x} = \boldsymbol{\omega}_{1,x0} + \frac{5}{7R_1(1+M)}(S_0\sin\theta_0) \tag{35}$$

$$\boldsymbol{\omega}_{1,y} = \boldsymbol{\omega}_{1,y0} - \frac{5}{7R_1(1+M)}(S_0\cos\theta_0) \tag{36}$$

$$\boldsymbol{\omega}_{1,z} = \boldsymbol{\omega}_{1,z0} \tag{37}$$

For particle 2:

$$\mathbf{U}_{2,x} = \mathbf{U}_{2,x0} + \frac{2M}{7(1+M)}(S_0\cos\theta_0) \tag{38}$$

$$\mathbf{U}_{2,y} = \mathbf{U}_{2,y0} + \frac{2M}{7(1+M)}(S_0\sin\theta_0) \tag{39}$$

$$\mathbf{U}_{2,z} = \mathbf{U}_{2,z0} + \frac{M(1+e)}{(1+M)} C_0 \tag{40}$$

$$\boldsymbol{\omega}_{2,x} = \boldsymbol{\omega}_{2,x0} + \frac{5M}{7R_2(1+M)}(S_0\sin\theta_0) \tag{41}$$

$$\boldsymbol{\omega}_{2,y} = \boldsymbol{\omega}_{2,y0} - \frac{5M}{7R_2(1+M)}(S_0\cos\theta_0) \tag{42}$$

$$\boldsymbol{\omega}_{2,z} = \boldsymbol{\omega}_{2,z0} \tag{43}$$

Here, $M = m_1/m_2$ is the ratio of the particle masses.

(b) $f = \tan\alpha' < \tan\gamma$: The image point follows the curve described by Eq. (28) from Q_0 to Q_2 where the approach phase ends and continues to termination of impact at Q_3. The impulses at termination are:

$$\mathbf{P}_{z,3} = \left(\frac{m_1 m_2}{m_1+m_2}\right) C_0(1+e) \tag{44}$$

$$\mathbf{P}_{x,3} = f\cos\theta_0\left(\frac{m_1 m_2}{m_1+m_2}\right) C_0(1+e) \tag{45}$$

$$\mathbf{P}_{y,3} = f\sin\theta_0\left(\frac{m_1 m_2}{m_1+m_2}\right) C_0(1+e) \tag{46}$$

It is assumed that the sliding direction is a constant, θ_0. The final velocities in this case are given as follows.

For particle 1:

$$\mathbf{U}_{1,x} = \mathbf{U}_{1,x0} - f\cos\theta_0 \frac{1+e}{1+M} C_0 \tag{47}$$

$$\mathbf{U}_{1,y} = \mathbf{U}_{1,y0} - f\sin\theta_0 \frac{1+e}{1+M} C_0 \tag{48}$$

$$\mathbf{U}_{1,z} = \mathbf{U}_{1,z0} - \frac{1+e}{1+M} C_0 \tag{49}$$

$$\boldsymbol{\omega}_{1,x} = \boldsymbol{\omega}_{1,x0} + f\sin\theta_0 \frac{5(1+e)}{2R_1(1+M)} C_0 \tag{50}$$

$$\boldsymbol{\omega}_{1,y} = \boldsymbol{\omega}_{1,y0} - f\cos\theta_0 \frac{5(1+e)}{2R_1(1+M)} C_0 \tag{51}$$

$$\boldsymbol{\omega}_{1,z} = \boldsymbol{\omega}_{1,z0} \tag{52}$$

For particle 2:

$$\mathbf{U}_{2,x} = \mathbf{U}_{2,x0} + f\cos\theta_0 \frac{M(1+e)}{1+M} C_0 \tag{53}$$

$$\mathbf{U}_{2,y} = \mathbf{U}_{2,y0} + f\sin\theta_0 \frac{M(1+e)}{1+M} C_0 \tag{54}$$

$$\mathbf{U}_{2,z} = \mathbf{U}_{2,z0} + \frac{M(1+e)}{1+M} C_0 \tag{55}$$

$$\boldsymbol{\omega}_{2,x} = \boldsymbol{\omega}_{2,x0} + f\sin\theta_0 \frac{5M(1+e)}{2R_2(1+M)} C_0 \tag{56}$$

$$\boldsymbol{\omega}_{2,y} = \boldsymbol{\omega}_{2,y0} - f\cos\theta_0 \frac{5M(1+e)}{2R_2(1+M)} C_0 \tag{57}$$

$$\boldsymbol{\omega}_{2,z} = \boldsymbol{\omega}_{2,z0} \tag{58}$$

2.3. The collision mechanism

The fluid–particle solver is described in detail in [10] and basic steps are recounted briefly in the next section. In this section, we discuss the relevant steps where the collision model is implemented in the overall scheme of the algorithm.

The collision mechanism has two functions to perform; first is detection of collision and second correcting particle velocities in case of collision. At every time step, the collision detection function checks for collision between any two particles at the position predicted by [10, Eq. (17)] and again after the final particle positions are updated by [10, Eq. (28)]. This ensures that at the completion of every time step, no particle domains are overlapping. The collision detection declares collision under the following conditions:

- The gap between the colliding surfaces is taken as:

$$h_0 = \begin{cases} |\mathbf{X}_1 - \mathbf{X}_2| - (R_1 + R_2), & \text{collision with particle} \\ |\mathbf{X}_1 - \mathbf{X}_w| - R_1, & \text{collision with wall} \end{cases}$$

  where $\mathbf{X}_w$ is the point on the wall closest to the particle, in other words the value of $|\mathbf{X}_1 - \mathbf{X}_w|$ can be obtained by distance of a point (in this case center of the particle) to plane formula. If the gap is less than one grid spacing then the particle(s) are considered for collision correction.
- A first order accurate prediction of the position of particles is made using current particle velocities at next time step and if the gap at these predicted positions is negative, then the particles are considered for collision correction in current time step itself.

The collision detection function returns whether the particle under consideration is colliding with another particle or bounding walls or both. Only in case of collision, the correction of particle velocities is applied following the steps below:

- A local co-ordinate system is defined at the point of contact as shown in Fig. 1. The z-axis or the axis of compression is specified along the normal from particle-1 to particle-2. There are infinitely many ways to specify other two axes in the tangent plane. We resolve the velocity of the first particle along the normal and perpendicular to this normal. This perpendicular direction is taken as x-axis and the y-axis is taken perpendicular to both x- and z-axes. This means that particle-1 will never have any velocity component along the y-axis.
- All the translational and angular velocities of both particles are transformed to this local co-ordinate system.
- Now the sliding and compression velocities are found using (17). The magnitude of sliding and compression velocities is calculated and the angle of sliding is calculated.
- Next the Stokes number as defined by (4) and the value of coefficient of restitution as defined by (2) is calculated.
- To determine whether the friction acts at its limiting value, the critical angle as defined in (27) is calculated.
- If the friction coefficient $f = \tan\alpha > \tan\gamma$, the set of Eqs. (32)–(37) and (38)–(43) is applied. Otherwise, the second set (47)–(52) and (53)–(58) is applied.

The collision with wall is treated similarly, with the assumption that the wall is massive, i.e. $m_2 \to \infty$ which implies putting $M = 0$ in all the expressions. The entire collision detection and velocity correction procedure is implemented inside a loop with sub-time stepping to afford better collision detection.

3. Results and discussion

The collision model is used in the particle position prediction and correction steps of our particulate flow formulation presented in [10]. It is based on the fictitious domain approach and includes the following basic steps:

Table 1
Materials used and the corresponding simulation parameters

Material	ρ_p	*Re*	*St*
PVC	1410.0	31.4648	4.0811
Teflon	2160.0	91.7935	18.2388
Steel	7830.0	311.1846	224.1352
Brass	8530.0	330.5544	259.3714

- Advection of the fluid velocity and prediction of the particles positions.
- Diffusion of the fluid velocity.
- Imposition of the incompressibility constraint via a second order pressure-correction scheme.
- Imposition of the rigid body motion within the domain occupied by the particles via a fictitious domain approach. It allows to significantly simplify the overall formulation and solve the problem in simplified domains, that include the particles, and allows for an easier parallelization.
- Correction of the particles positions.

The spatial discretization is based on second-order $P_2 - P_1$ finite elements. Here we present the results obtained in three different numerical experiments where the collision model was employed.

3.1. Settling particle interaction with neutrally buoyant particle

Settling particles of different materials were used to vary the density ratio with respect to the fixed fluid medium.

Table 1 gives details of the parameters used in the numerical study. The fluid medium used was 80% glycerine solution at 21 °C. The viscosity of this solution is 57.48 cP and density is 1.208 g/cc. The diameter of the settling particle is 1.27 cm and that of neutrally buoyant particle is 2.54 cm. The dimensions of the container are $8.1 \times 6.1 \times 4.1$ cm.

Fig. 3 shows the sequence of interaction of the settling and neutrally buoyant particle and Fig. 4, we show the positions of the settling and neutrally buoyant particles as collision proceeds. The initial position of settling and neutrally buoyant particles are shown by circles. The two side figures show the enlarged trajectory of neutrally buoyant particle and the interaction of the settling particle with bottom wall. The denser settling particles leave contact sooner and the brass particle can be seen to bounce at the bottom wall.

3.2. Drafting, kissing and tumbling mechanism

This is a well known phenomenon for interaction between two settling particles [11]. The settling particles used in this experiment were PVC particles of diameter 1.27 cm. Initially they were placed vertically one d_p apart with the top particle offset by a small distance $(0.1d_p)$ in positive z-direction to predefine the tumbling plane. The channel used has a square cross-section of side 5.08 cm and length of the channel is 25.4 cm. The sequence of drafting, kissing and tumbling is shown in Fig. 5. Fig. 6 shows the velocity of the settling particles.

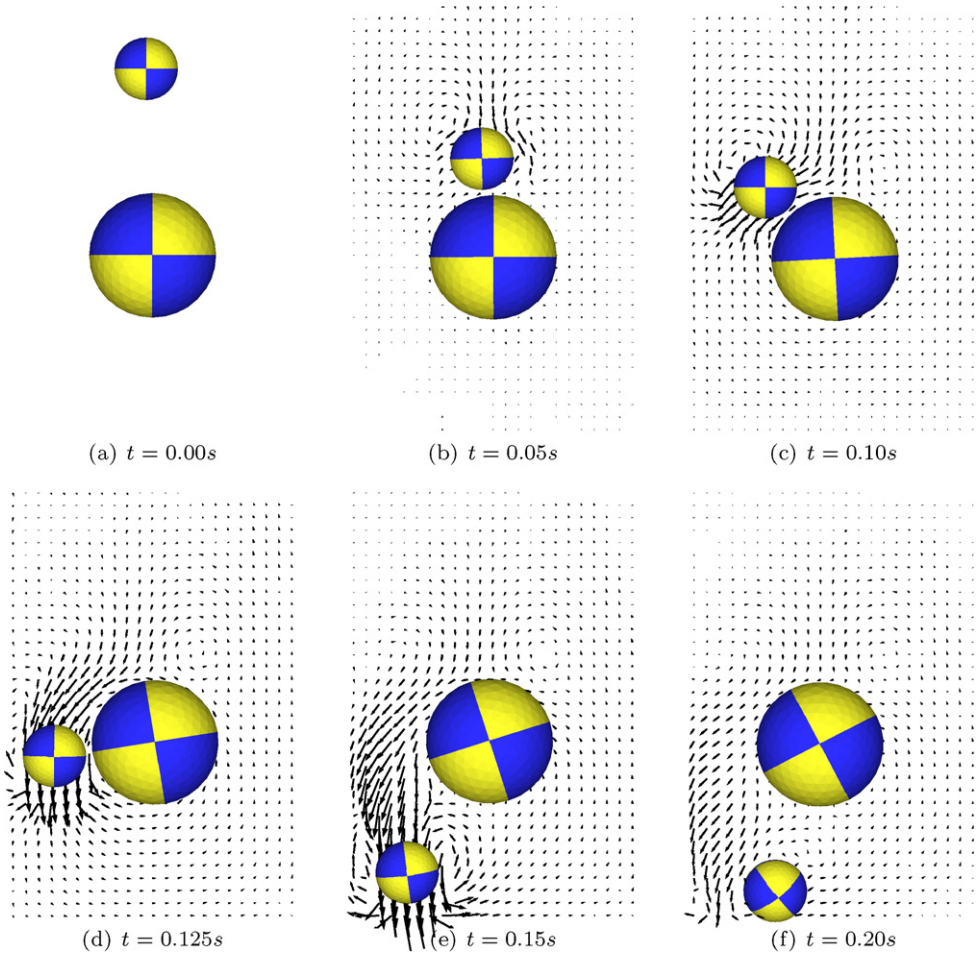

Fig. 3. Interaction of settling and neutrally buoyant particles.

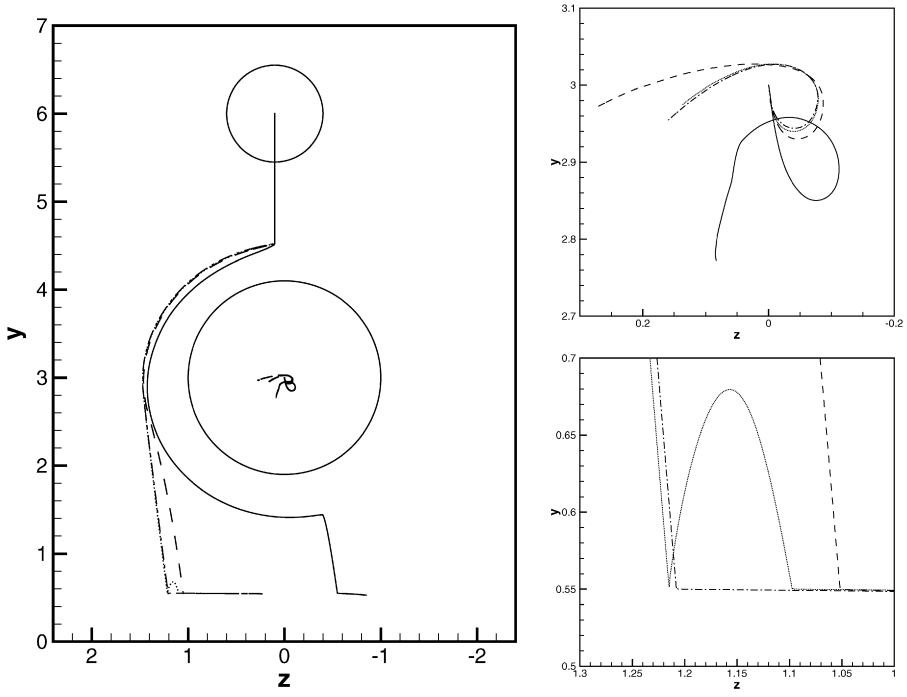

Fig. 4. Trajectory of the particles: solid line—PVC, dashed—Teflon, dashed dot—steel and dotted—brass particle.

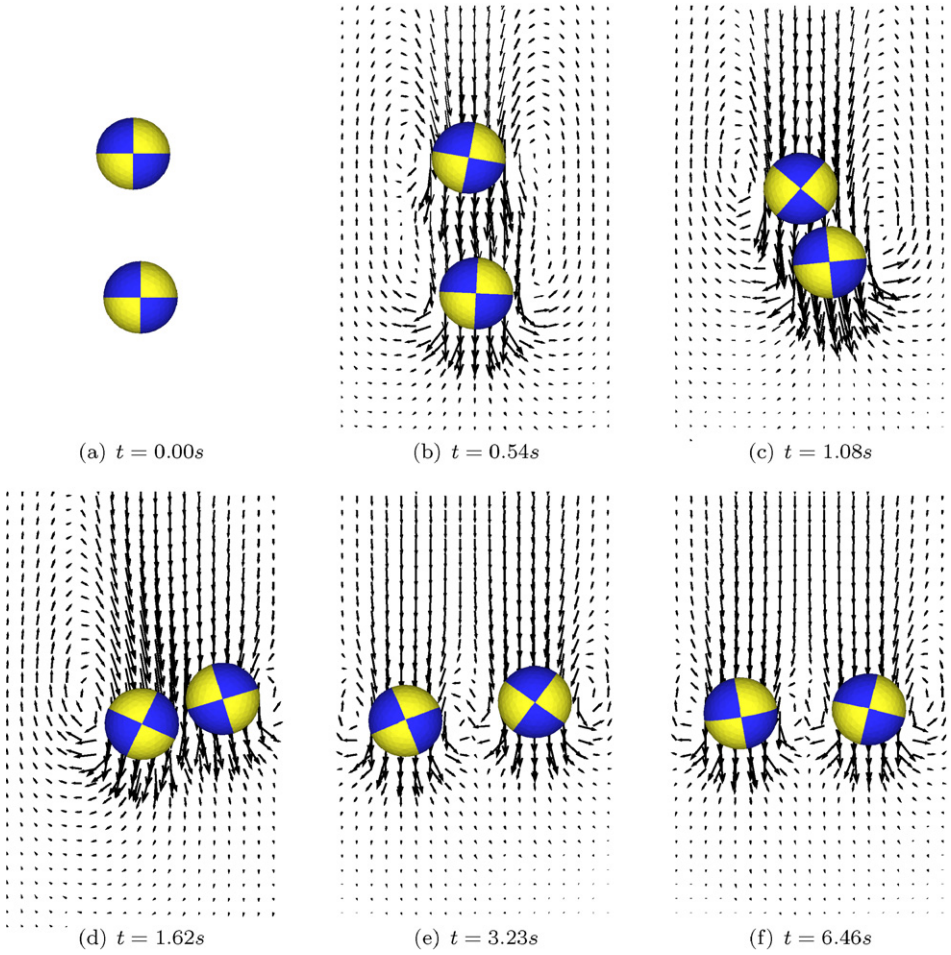

Fig. 5. Drafting–kissing–tumbling sequence of two settling particles.

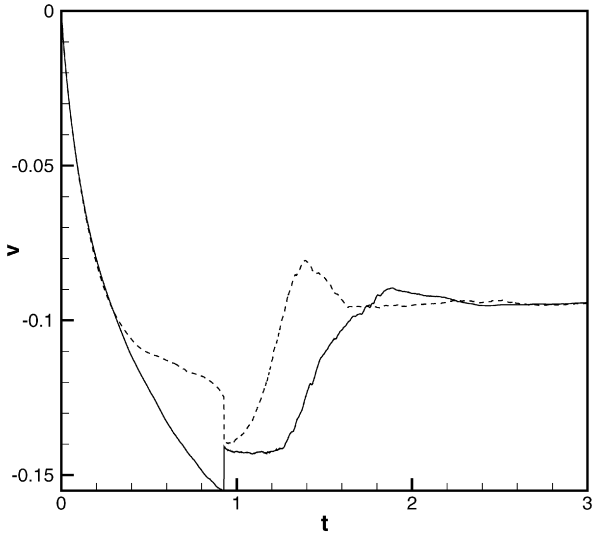

Fig. 6. Trajectory of the two settling particles undergoing drafting, kissing and tumbling mechanism.

3.3. Simulation of 64 particles

The collision model developed is for two particle interaction, however it can be easily extended to large number of particles using time substepping. Fig. 7 shows frames of the settling of 64 particles in closed box taken at specific time steps. The particles are initially arranged in a cubic array of $4 \times 4 \times 4$ particles at the top of the box and then let to settle. Initially the particles settle in a wave-like fashion with expansion of the cluster. As the particles at the center start to accelerate, they create low pressure in the wake and other particles are drawn into the wake leading to creation of swirls. The higher the density of the particles with respect to the fluid, the sooner the cluster breaks into swirls. The density ratio in the present case is $\rho_p/\rho = 7.06$.

4. Conclusion

A collision model based on stereomechanical impact theory is developed for particle–particle and particle–wall interaction inside viscous medium. The coefficient of restitution is used as a function of Stokes number which captures the ratio of particle inertia to the viscous force of fluid. The coefficient of friction is used as suggested in [4]. A number of numerical tests were performed on the model to qualitatively verify the physics captured by the model. Further experiments are required to validate the model for the various cases presented.

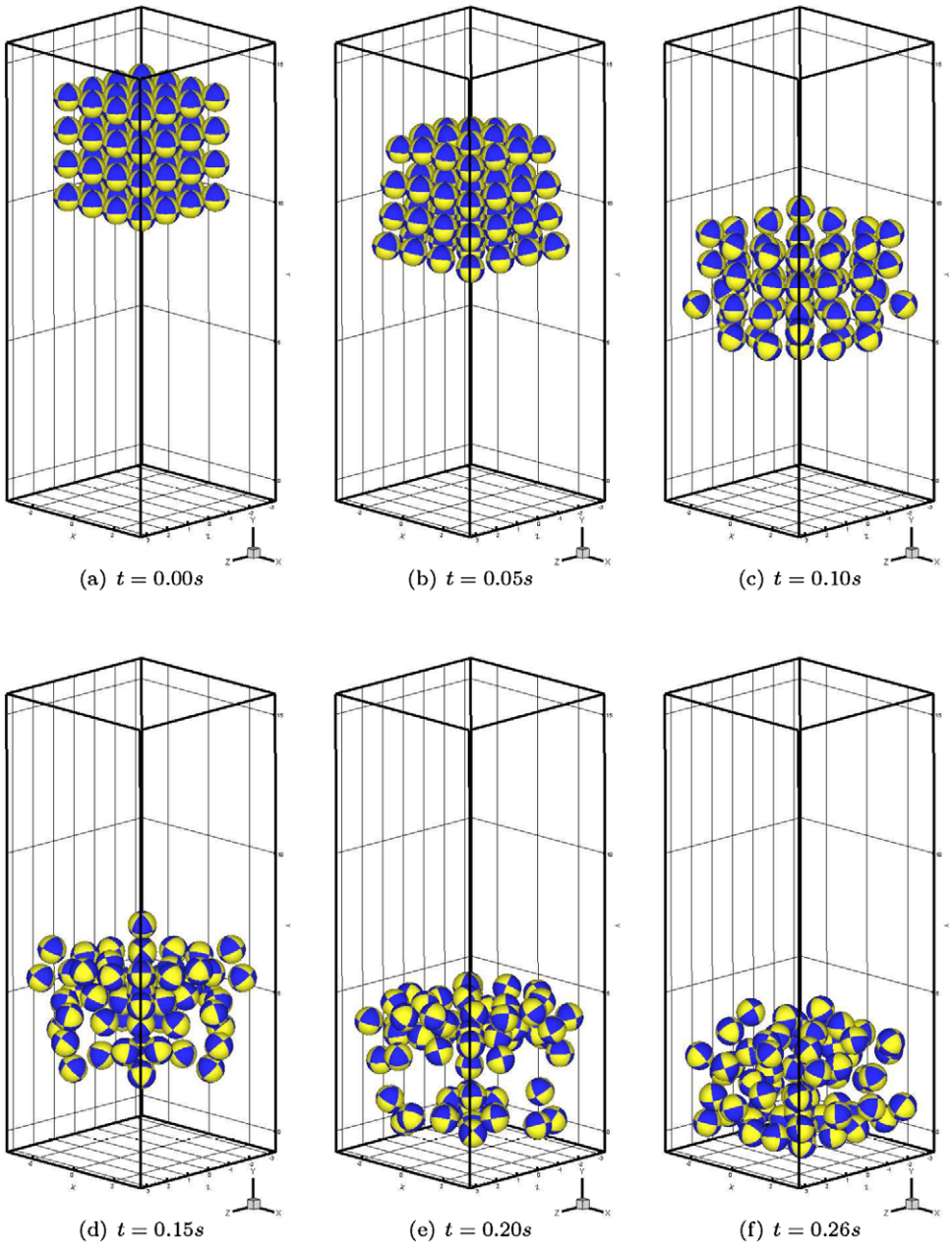

Fig. 7. Sedimentation of 64 spherical particles in a 3D closed box.

Acknowledgements

This study has been supported by Discovery Grants of the National Science and Engineering Research Council of Canada (NSERC).

References

[1] J.R. Smart, D.T. Leighton, Measurement of the hydrodynamic surface roughness of non-colloidal spheres, Physics of Fluids 1 (1989) 52–60.
[2] R.H. Davis, Effects of surface roughness on a sphere sedimenting through a dilute suspension of neutrally buoyant spheres, Physics of Fluids A 4 (12) (1992) 2607–2619.
[3] W. Goldsmith, Impact: The Theory and Physical Behaviour of Colliding Solids, Edward Arnold Ltd., London, 1960.
[4] F.L. Yang, M.L. Hunt, Dynamics of particle–particle collisions in a viscous liquid, Physics of Fluids 18 (121506) (2006) 1–11.
[5] G.G. Joseph, R. Zenit, M.L. Hunt, A.M. Rosenwinkel, Particle wall collisions in a viscous fluid, Journal of Fluid Mechanics 433 (2001) 329–346.
[6] G.G. Joseph, M.L. Hunt, Oblique particle-wall collisions in a liquid, Journal of Fluid Mechanics 510 (2004) 71–93.
[7] R.H. Davis, J.M. Serayssol, E.J. Hinch, The elastohydrodynamic collision of two spheres, Journal of Fluid Mechanics 163 (1986) 479–497.
[8] A.A. Kantak, R.H. Davis, Oblique collisions and rebound of spheres from a wetted surface, Journal of Fluid Mechanics 509 (2004) 63–81.
[9] P. Gondret, M. Lance, L. Petit, Bouncing motion of spherical particles in fluids, Physics of Fluids 14 (2) (2002) 643–652.
[10] C. Veeramani, P.D. Minev, K. Nandakumar, A fictitious domain formulation for flows with rigid particles: A non-Lagrange multiplier version, Journal of Computational Physics 224 (2007) 867–879.
[11] A.F. Fortes, D.D. Joseph, T.S. Lundgren, Nonlinear mechanics of fluidization of beds of spherical particles, Journal of Fluid Mechanics 177 (1987) 467–483.